JACS
JOURNAL OF THE AMERICAN CHEMICAL SOCIETY
Article
pubs.acs.org/JACS

Side-Chain Isomerization on an n-type Organic Semiconductor ITIC Acceptor Makes 11.77% High Efficiency Polymer Solar Cells

Yankang Yang,[†,§] Zhi-Guo Zhang,*[,†] Haijun Bin,[†,§] Shanshan Chen,[‡] Liang Gao,[†,§] Lingwei Xue,[†] Changduk Yang,[‡] and Yongfang Li*[,†,§,∥]

[†]Beijing National Laboratory for Molecular Sciences, CAS Key Laboratory of Organic Solids, Institute of Chemistry, Chinese Academy of Sciences, Beijing 100190, China

[‡]Department of Energy Engineering, School of Energy and Chemical Engineering, Low Dimensional Carbon Materials Center, Ulsan National Institute of Science and Technology (UNIST), Ulsan 689-798, South Korea

[§]University of Chinese Academy of Sciences, Beijing 100049, China

[∥]Laboratory of Advanced Optoelectronic Materials, College of Chemistry, Chemical Engineering and Materials Science, Soochow University, Suzhou, Jiangsu 215123, China

Supporting Information

ABSTRACT: Low bandgap n-type organic semiconductor (n-OS) ITIC has attracted great attention for the application as an acceptor with medium bandgap p-type conjugated polymer as donor in nonfullerene polymer solar cells (PSCs) because of its attractive photovoltaic performance. Here we report a modification on the molecular structure of ITIC by side-chain isomerization with *meta*-alkyl-phenyl substitution, *m*-ITIC, to further improve its photovoltaic performance. In a comparison with its isomeric counterpart ITIC with *para*-alkyl-phenyl substitution, *m*-ITIC shows a higher film absorption coefficient, a larger crystalline coherence, and higher electron mobility. These inherent advantages of *m*-ITIC resulted in a higher power conversion efficiency (PCE) of 11.77% for the nonfullerene PSCs with *m*-ITIC as acceptor and a medium bandgap polymer J61 as donor, which is significantly improved over that (10.57%) of the corresponding devices with ITIC as acceptor. To the best of our knowledge, the PCE of 11.77% is one of the highest values reported in the literature to date for nonfullerene PSCs. More importantly, the *m*-ITIC-based device shows less thickness-dependent photovoltaic behavior than ITIC-based devices in the active-layer thickness range of 80−360 nm, which is beneficial for large area device fabrication. These results indicate that *m*-ITIC is a promising low bandgap n-OS for the application as an acceptor in PSCs, and the side-chain isomerization could be an easy and convenient way to further improve the photovoltaic performance of the donor and acceptor materials for high efficiency PSCs.

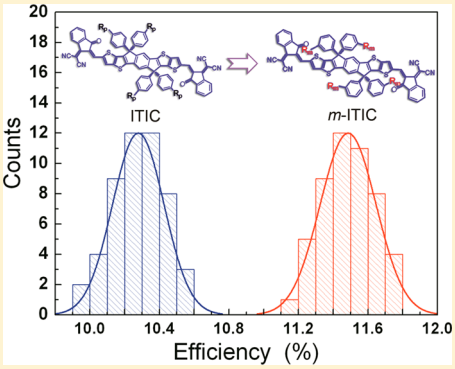

INTRODUCTION

Polymer solar cells (PSCs), containing a phase-separated bicontinuous network of a p-type conjugated polymer as donor and an n-type fullerene derivative as acceptor, have been intensively investigated to take their advantages of light weight, flexibility, low production cost, and suitability for large-scale production.[1−5] At present, state-of-the-art PSCs have already exhibited power conversion efficiencies (PCEs) of up to 10−11%.[6−10] However, the intrinsic drawbacks of fullerene acceptors, such as difficulty to tune energy levels, poor visible light absorption, and inherent tendency of easy aggregation, make it difficult to further improve photovoltaic performance of the PSCs. Thus, nonfullerene acceptors, with synthetic flexibility and great potential to overcome the above-mentioned drawbacks of the fullerene acceptors, aroused intense interest.[11−41]Among the nonfullerene acceptors, a variety of n-type conjugated polymers containing strong electron deficient groups, such as B ← N bridged bipyridine[11] and aromatic diimide (such as perylene diimide,[12−14] naphthalene diimide,[15−19] and naphthodithiophene diimide[20]), are explored as polymer acceptors. Also, n-type organic semiconductors (n-OSs) such as A−D−A (acceptor−donor−acceptor) structured n-OSs,[21−23] rylene diimide (perylene diimide,[24−31] naphthalene diimide,[32] tetraazabenzodifluoroanthene diimide[33,34])- and diketopyrrolopyrrole-[35−37] based n-OSs are successfully used in the nonfullerene PSCs.

Low bandgap A−D−A structured n-OSs are in particular interesting for harvesting light in the visible−near-infrared region and thus hold great promise to construct high efficiency PSCs. Especially, the fused-aromatic-ring-based n-OS ITIC developed by Zhan et al.[38] attracted great attention for the application as acceptor in nonfullerene PSCs recently.[38,42−44] ITIC possesses a suitable LUMO energy level of ca. −3.8 eV

Received: August 30, 2016
Published: October 25, 2016

DOI: 10.1021/jacs.6b09110
J. Am. Chem. Soc. 2016, 138, 15011−15018

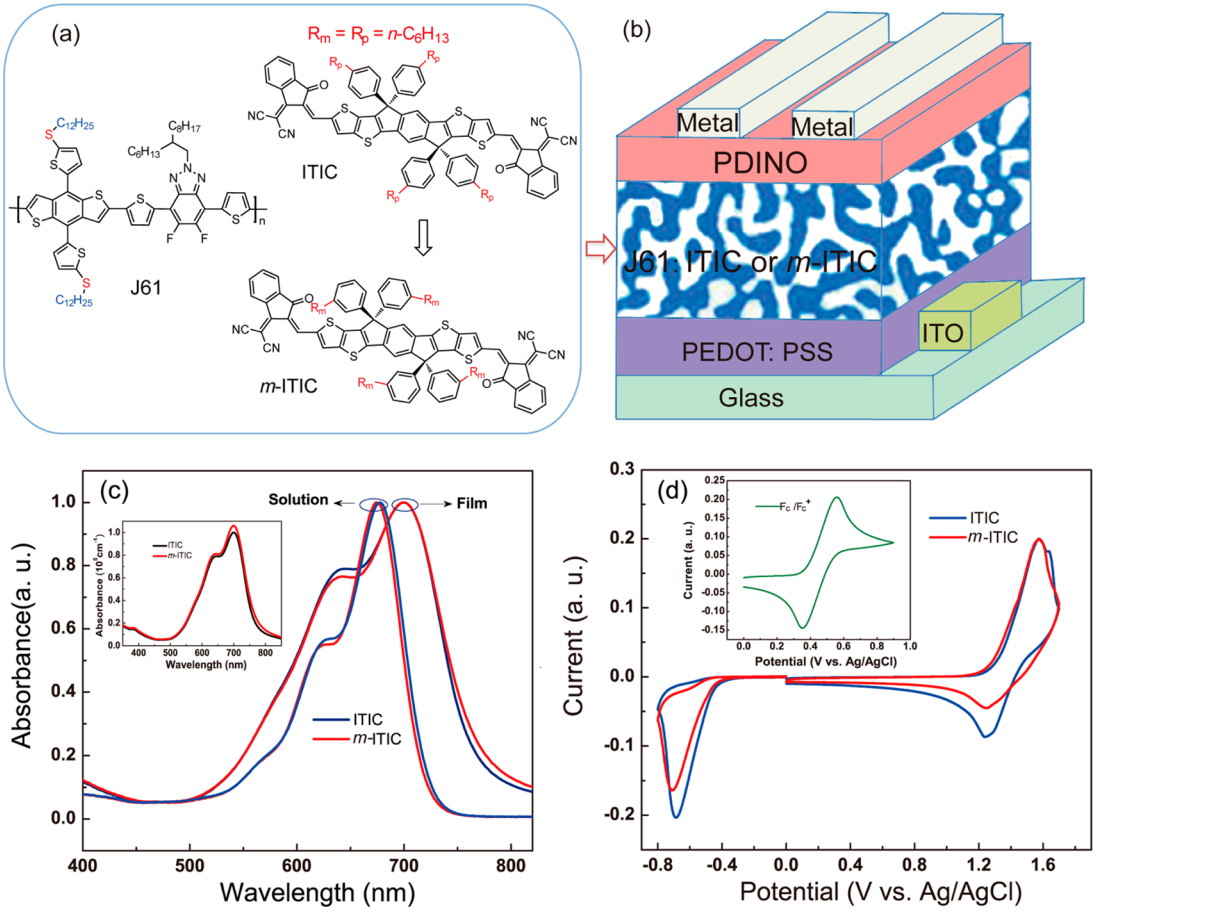

Figure 1. (a) Molecular structures of J61 polymer donor and the n-OSs (ITIC and *m*-ITIC) acceptors. (b) Device structure of the nonfullerene PSCs used in this work. (c) Solution and film absorption spectra of ITIC and *m*-ITIC; the inset shows the absorption coefficient of ITIC and *m*-ITIC in film state. (d) Cyclic voltammograms of ITIC (blue line) and *m*-ITIC (red line); the inset shows the cyclic voltammogram of ferrocene/ferrocenium (Fc/Fc^+) couple used as an internal reference.

Scheme 1. Synthetic Route of *m*-ITIC

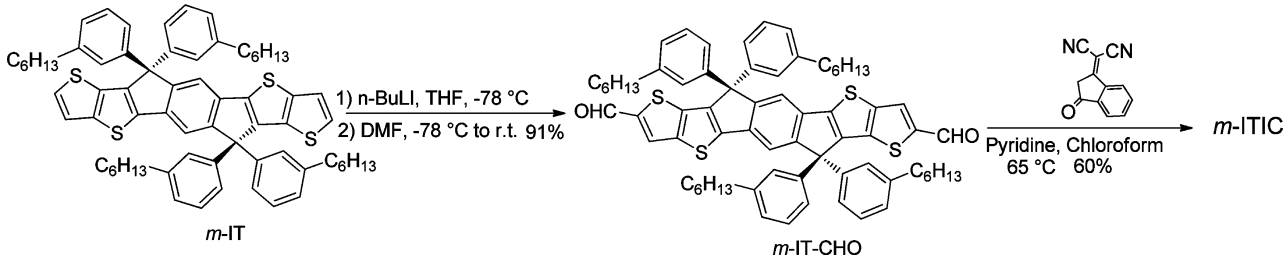

and a narrower bandgap of 1.59 eV with strong absorption from 500 to 780 nm. Meanwhile, the steric effect of its alkyl-phenyl substituents can prevent $\pi-\pi$ aggregation of ITIC molecules to ensure solubility for solution processing and appropriate aggregation in the blend films with conjugated polymer donor. All of these desirable characteristics enabled high PCEs of 9−11% for the nonfullerene PSCs with ITIC as acceptor and medium bandgap conjugated polymers as donor.[42−44] The success of the ITIC inspired tremendous efforts focusing on manipulating the aromatic core,[45] the bridge,[46] the end-capping electron deficient groups,[40,47] as well as the aromatic side-chain[48] in an effort to fine-tune the band gap and energy levels by changing the intramolecular electronic coupling. However, no attention has been paid to the flexible side-chain engineering on the low bandgap n-OS ITIC with *para*-alkyl-phenyl substituents. Actually, alternation of flexible side-chains in shape, length, and branch position has a significant impact on intermolecular self-assembly of the conjugated polymers and organic semicondutors.[23,49−57] In the PSCs, intermolecular self-assembly of the active-layer components is one of the crucial factors that govern the film morphology and thereby device performance. On the basis of these considerations, herein, we performed side-chain engineering on the high performance n-OS ITIC, synthesized an isomer of ITIC with *meta*-alkyl-phenyl substitution, *m*-ITIC (see Figure 1), and investigated its photovoltaic properties in combination with our recently developed medium bandgap conjugated polymer J61[43] (2D-conjugated benzodithiophene-alt-fluorobenzotriazole copolymer with alkylthio side-chain) as donor. PCE of the PSCs based on J61/*m*-ITIC reached 11.77%,

DOI: 10.1021/jacs.6b09110
J. Am. Chem. Soc. 2016, 138, 15011−15018

Table 1. Comparison of the Crystallinity, Thermal and Physicochemical Properties, and Electron Motilities of the Two n-OSs

n-OSs	d[100] (Å)	CCL[100] (Å)[a]	d[010] (Å)	CCL[010][a] (Å)	T_d[b] (°C)	λ_{edge}[c] (nm)	E_g^{opt}[d] (eV)	E_{LUMO}[e] (eV)	E_{HOMO}[e] (eV)	μ_e [10^{-4}cm^2 V^{-1} s^{-1}]
ITIC	18.2	38.5	3.7	19.6	350.1	782	1.59	−3.84	−5.54	1.60
m-ITIC	23.2	110.9	3.7	46.9	338.7	784	1.58	−3.82	−5.52	2.45

[a]Calculated from Scherrer equation: CCL = $2\pi K/\Delta q$, where Δq is the full-width at half-maximum of the peak and K is a shape factor (0.9 was used here). [b]5% weight-loss temperature measured by TGA under nitrogen. [c]Absorption edge of the polymer films. [d]Calculated from the absorption edge of the polymer films: $E_g^{opt} = 1240/\lambda_{edge}$. [e]Calculated according to the equation $E_{LUMO/HOMO} = -e(E_{red/ox} + 4.36)$ (eV).

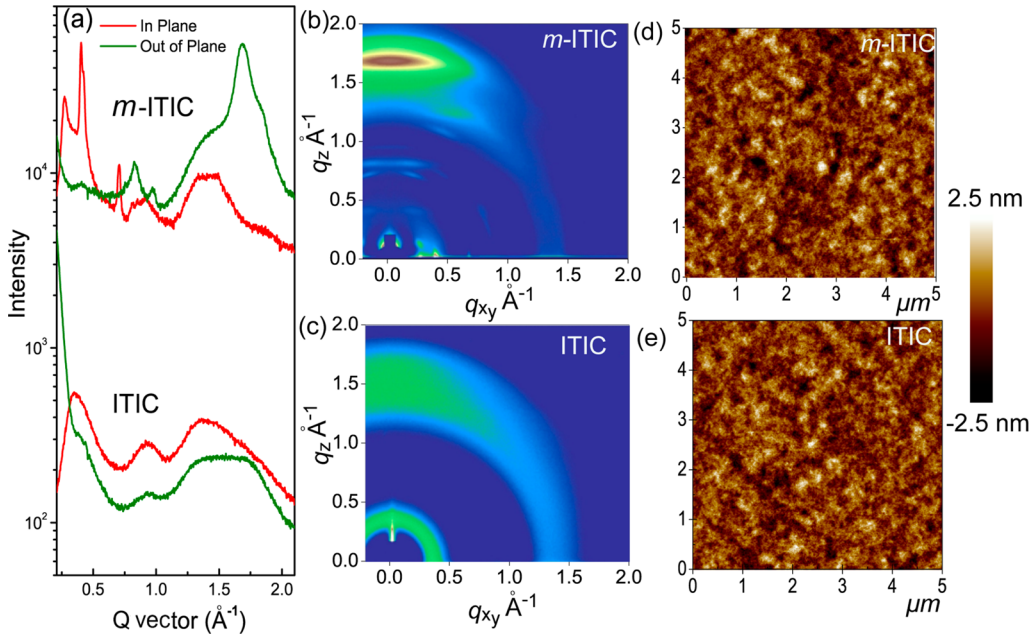

Figure 2. (a) Line cuts of the GIWAXS images of ITIC film and *m*-ITIC film; GIWAXS images of the (b) *m*-ITIC film and (c) ITIC film. Representative AFM height images of (d) *m*-ITIC and (e) ITIC films.

which is improved over that (10.57%) of the corresponding PSCs with ITIC as acceptor. To the best of our knowledge, this PCE of 11.77% is one of the highest values reported in the literature to date for nonfullerene PSCs.

RESULTS AND DISCUSSION

Synthesis and Characterization. Chemical structure of ***m*-ITIC** is shown in Figure 1a and corresponding synthetic routes are depicted in Scheme 1. The synthesis of indacenodithieno[3,2-*b*]thiophene (*m*-IT) has been well described by Wang and used as donor building block in p-type polymers.[58] For the synthesis of *m*-ITIC, *m*-IT was initially converted into its corresponding aldehyde *m*-IT-CHO by lithiation with *n*-butyllithium followed by quenching with dimethylformamide (DMF). Knoevenagel condensation of *m*-IT-CHO with 2-(3-oxo-2,3-dihydroinden-1-ylidene)-malononitrile afforded the new n-OS *m*-ITIC.

Both ITIC and *m*-ITIC were found to have almost the same film absorption profile (see Figure 1c), showing the main absorption peak at ca. 700 nm and absorption edge at 782 nm regardless of the chosen side-chains. However, with the *meta*-alkyl-phenyl substitution, the *m*-ITIC film displays obviously improved light harvesting properties with higher film absorption coefficient of 1.06×10^5 cm^{-1} at 700 nm relative to that of ITIC (1.00×10^5 cm^{-1}), suggesting its stronger light harvest ability.

The thermal stability of the two n-OSs was evaluated by thermogravimetric analysis (TGA), as shown in Figure S1 in the Supporting Information (SI). The thermal decomposition temperatures (T_d's) at 5% weight loss (see Table 1) are 350.1 and 338.7 °C for ITIC and *m*-ITIC, respectively. The T_d values indicate that the thermal stabilities of the two n-OSs are high enough for their application in PSCs.

The electronic energy levels of the n-OSs were measured by electrochemical cyclic voltammetry[59,60] with Ag/AgCl as reference electrode and Fc/Fc$^+$ couple as an internal reference. Figure 1d shows the cyclic voltammograms of *m*-ITIC and ITIC films. From the onset oxidation potential (E_{ox}) and onset reduction potential (E_{red}), the highest occupied molecular orbital (HOMO) energy level (E_{HOMO}) and the lowest unoccupied molecular orbital (LUMO) energy level (E_{LUMO}) were determined according to the equation $E_{LUMO/HOMO} = -e(E_{red/ox} + 4.36)$ (eV). (Redox potential of Fc/Fc$^+$ is 0.44 V vs Ag/AgCl in our measurement system, and we take the energy level of Fc/Fc$^+$ as 4.8 eV below vacuum.) The LUMO and HOMO energy levels of *m*-ITIC are −3.82 and −5.52 eV, respectively (Table 1), which are similar to those of ITIC. Thus, it appears that manipulating the alkyl-chain attaching point has little effect on E_{HOMO} and E_{LUMO}. It should be mentioned that the slightly different oxidation/re-reduction reversibility of ITIC and *m*-ITIC in the cyclic voltammograms could be due to the effect of the different side-chain conformation on the related charge transfer processes.

One dramatic effect of the side-chain position is on the crystallinity and molecular organization in the n-OS thin films, which is evidenced by grazing incident wide-angle X-ray diffraction (GIWAXS)[61] as shown in Figure 2a–c. For ITIC, both the lamellar (100) reflections (at 0.35 Å^{-1}) and π–π

DOI: 10.1021/jacs.6b09110
J. Am. Chem. Soc. 2016, 138, 15011–15018

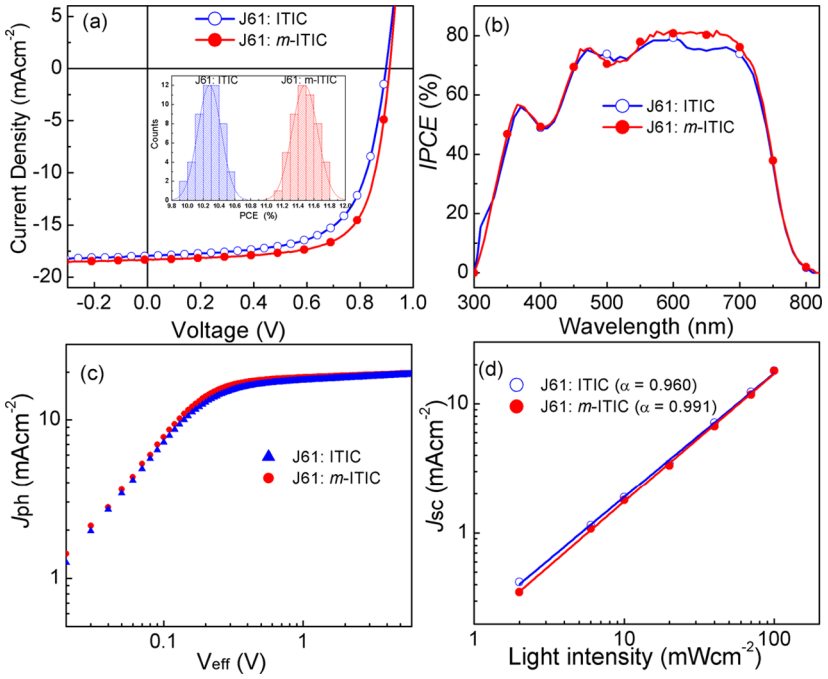

Figure 3. (a) $J-V$ curves of the champion devices with D/A weight ratio of 1:1 and thermal annealing at 130 °C for 5 min under the illumination of AM 1.5G, 100 mW cm^{-2}; the inset shows the histogram of the PCE counts for 50 devices. (b) IPCE spectra of the champion devices with D/A weight ratio of 1:1 and thermal annealing at 130 °C for 5 min. (c) J_{ph} versus V_{eff} of the optimized devices. (d) Light intensity dependence of J_{sc}.

Table 2. Photovoltaic Parameters of the Devices Based on J61:ITIC and J61:*m*-ITIC with D/A Weight Ratio of 1:1 and Thermal Annealing at 130 °C for 5 min under the Illumination of AM1.5G, 100 mW/cm^2

acceptor	V_{oc} [V]	J_{sc} [mA cm^{-2}]	FF [%]	PCE [%]	R_s[a] [Ω cm^2]	R_{sh}[b] [kΩ cm^2]	μ_h/μ_e
ITIC	0.898 (0.900 ± 0.004)	17.97 (17.72 ± 0.45)	65.49 (64.55 ± 1.38)	10.57 (10.28 ± 0.15)	8.81 (9.03 ± 0.43)	0.96 (1.26 ± 0.56)	1.97
m-ITIC	0.912 (0.902 ± 0.004)	18.31 (18.31 ± 0.34)	70.55 (69.55 ± 1.10)	11.77 (11.49 ± 0.16)	6.74 (7.63 ± 0.49)	1.47 (1.52 ± 0.37)	1.18

[a]Calculated from the inverse slope at $V = V_{OC}$ in $J-V$ curves under illumination. [b]Calculated from the inverse slope at $V = 0$ in $J-V$ curves under illumination.

stacking (010) reflection (at 1.70 Å^{-1}) were competitively observed along the out-of-plane direction, confirming that face-on and edge-on crystallites coexisted. The relatively weak (010) $\pi-\pi$ stacking peak for a neat ITIC film is properly related to its slightly poor self-organization behavior with the *para*-alkyl-phenyl substitution. Thus, the crystal coherence length (CCL) in this direction obtained by the Scherrer equation is 19.6 Å. With changing position of the substitution, *m*-ITIC showed better defined scattering peaks and stronger intensities with a predominant face-on crystalline orientation, as shown by the clear and strong (100) diffraction in the in-plane direction (at 0.27 Å^{-1}) and $\pi-\pi$ stacking (010) diffraction (at 1.69 Å^{-1}) in the out-of-plane direction (Figure 2b). Interestingly, the CCL in the (010) direction is increased to 46.9 Å, implying that meta-arrangement of the alkyl-phenyl chains resulted in a significantly higher degree of self-organization and crystallinity.

The high crystalline feature in the *m*-ITIC film is also revealed by its larger root-mean-square (RMS) roughness of 0.953 ± 0.021 nm over that of the ITIC film (0.637 ± 0.053 nm) in the atomic force microscopy (AFM) images as shown in Figure 2d,e. The RMS values are averaged on the basis of testing five times on different areas for each sample. In addition, the electron mobility, determined by the space-charge-limited current (SCLC) method, of *m*-ITIC (2.45×10^{-4} cm^2 V^{-1} s^{-1}), is approximately one and a half times that of ITIC (1.60×10^{-4} cm^2 V^{-1} s^{-1}) (see Table 1). The higher electron mobility is a direct result of long-range order with more preference for face-on orientation across its thickness, as charge hopping through π-orbital overlapping in n-OSs is the dominated carrier transport mechanism. Thus, better device performance can be expected for our new n-OS.

Photovoltaic Properties. To understand the effect of the side-chain engineering on the photovoltaic performance of the n-OS acceptors, we fabricated the PSCs based on J61 as donor and *m*-ITIC or ITIC as acceptor with the traditional sandwich device structure, i.e., ITO (indium tin oxide)/PEDOT:PSS (poly(3, 4-ethylenedioxythiophene):poly(styrene-sulfonate))/J61:ITIC or *m*-ITIC/PDINO (perylene diimide functionalized with amino *N*-oxide)/Al, where PDINO was used to effectively alleviate the interfacial energy barriers.[62] For the choice of medium band gap polymer donor, we noticed some reports using P3HT as donor.[23,35,37] Here J61 was used as a polymer donor due to its special advantages such as 2D-conjugated structure, suitable HOMO energy level, proper crystallinity, and good photovoltaic performance in the nonfullerene PSCs with ITIC as acceptor.[43] The active layers were prepared by spin-coating the J61:ITIC or *m*-ITIC (1:1, w/w) blend solution with a total blend polymer concentration of 20 mg mL^{-1} in chloroform, followed by thermal annealing at 130 °C for 5 min. The optimized active-layer thickness was ca. 120 nm.

Figure 3a shows the current density–voltage ($J-V$) curves of the best devices with D/A weight ratio of 1:1 and thermal annealing at 130 °C for 5 min under the illumination of AM 1.5G, 100 mW/cm^2. Also, the log plots of the $J-V$ curves are

DOI: 10.1021/jacs.6b09110
J. Am. Chem. Soc. 2016, 138, 15011–15018

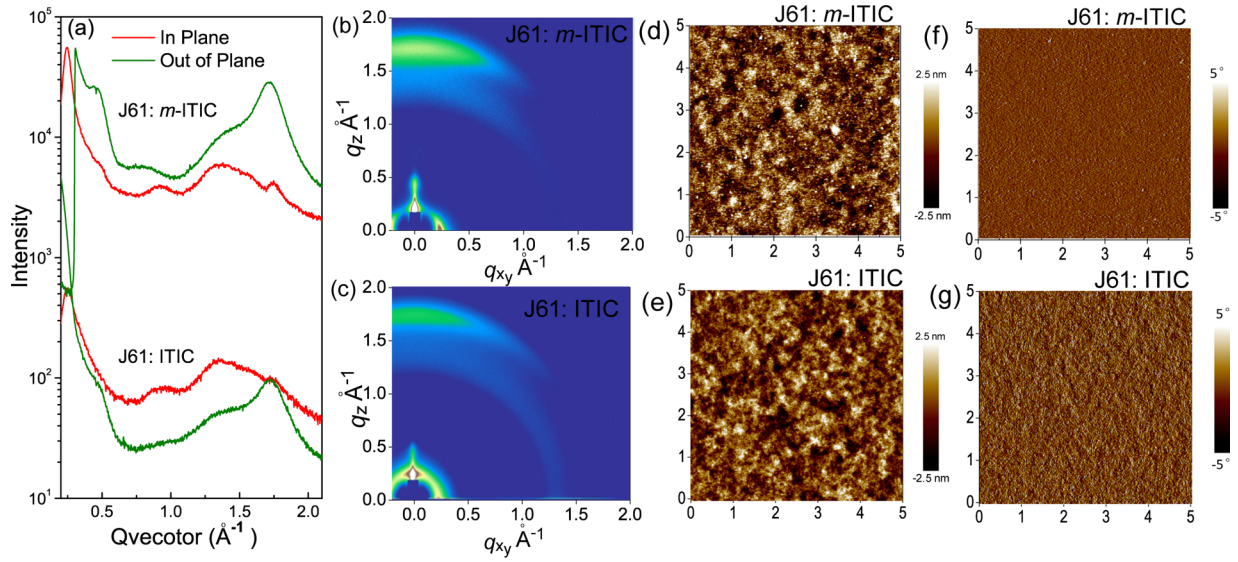

Figure 4. (a) Line cuts of the GIWAXS images of J61:ITIC (1:1, w/w) film and J61:*m*-ITIC (1:1, w/w) film. GIWAXS images of (b) J61:*m*-ITIC film and (c) J61:ITIC film. Representative AFM height images of (d) J61:*m*-ITIC (1:1, w/w) and (e) J61:ITIC (1:1, w/w) polymer blend films and corresponding AFM phase images of (f) J61:*m*-ITIC (1:1, w/w) and (g) J61:ITIC (1:1, w/w) polymer blend films.

provided in Figure S2 in SI, which indicate high quality of the diodes in the PSC devices. The photovoltaic performance data are listed in Table 2 for a clear comparison. The optimal PSCs based on J61:ITIC deliver a PCE of 10.57% with J_{sc} of 17.97 mA/cm^2, FF of 65.49% along with a V_{OC} of 0.898 V. The higher efficiency over our initial report[43] is primarily due to different thermal annealing conditions. Also, the correlation between thermal annealing temperature and device performance will be reported later. The *m*-ITIC-based devices showed a further improved PCE of 11.77% with a V_{OC} of 0.912 V, a J_{sc} of 18.31 mA/cm^2, and an FF of 70.55%. The significant improvements in the FF (70.55%) and J_{sc} (18.31 mA cm^{-2}) values of the *m*-ITIC-based device relative to those of the ITIC-based device (with FF of 65.49% and J_{sc} of 17.97 mA cm^{-2}) could be ascribed to the higher electron mobility of *m*-ITIC. To the best of our knowledge, the PCE of 11.77% is one of the highest values reported in the literature to date for single junction PSCs.

Figure 3b compares the IPCE spectra of the two devices with *m*-ITIC and ITIC as acceptor, respectively. The effect of the donor−acceptor complementary absorption strategy can be clearly illustrated from the high and broad photoresponse from 300 to 790 nm. The IPCE values in the shorter wavelength range of 300−550 nm, corresponding to the absorption of the polymer donor in the active layer, are almost the same for the two devices, which is reasonable because both devices use the same J61 polymer donor. Notably, for the photoresponse in the longer wavelength range 650−790 nm, which should be mostly ascribed to the contribution from the absorption of the acceptor component, the *m*-ITIC-based PSC demonstrated greater IPCE values than that of the ITIC-based device, indicating that the photon−electron conversion efficiency of the *m*-ITIC acceptor phase is higher than that of the ITIC acceptor phase in the devices. The integration of the IPCE values over the AM1.5G spectrum gave the current density value of 17.63 mA cm^{-2} for the *m*-ITIC-based devices and 17.13 mA cm^{-2} for the ITIC-based device, which agrees well with the J_{sc} values obtained from the *J*−*V* measurements (Table 2) within 5% mismatch.

To compare exciton dissociation and charge collection properties of the two PSCs with ITIC or *m*-ITIC as acceptor, we investigated the photocurrent density (J_{ph}) as a function of the effective voltage (V_{eff}) of the devices, as shown in Figure 3c. The photocurrent density J_{ph} is defined as $J_{ph} = J_L - J_D$, where J_L and J_D are the photocurrent densities under illumination and in the dark condition, respectively, and the effective voltage V_{eff} is defined as $V_{eff} = V_0 - V_{bias}$, where V_0 is the voltage at which J_{ph} is zero and V_{bias} is the applied external voltage bias. It can be seen from Figure 3c that J_{ph} is saturated (J_{sat}) at V_{eff} higher than 2 V, since the charge recombination is minimized at the higher voltage due to the high internal electric field in the device. The charge dissociation probability ($P(E, T)$) can be estimated from the value of the photocurrent density J_{ph} divided by the saturated photocurrent density (J_{sat}) (J_{ph}/J_{sat}). Under the short-circuit and maximal power output conditions, the $P(E,T)$ values are 97%, 81% for the device based on J61:ITIC, and 98%, 84% for the device based on J61:*m*-ITIC, respectively. The results indicate that the PSCs based on *m*-ITIC acceptor have a higher exciton dissociation rate and a more efficient charge collection relative to the PSCs based on the ITIC acceptor.

We further studied the effect of light intensity (P) on the short-circuit current density for understanding the charge recombination behavior of the PSCs, and the results are presented in Figure 3d. Generally, J_{sc} and P follow the relationship of $J_{sc} \propto P^{\alpha}$.[63] If all free carriers are swept out and collected at the electrodes prior to recombination, α should be equal to 1, while $\alpha < 1$ indicates some extent of bimolecular recombination. The α value of the ITIC-based device is 0.96, which indicates the existence of some extent of bimolecular recombination. While for *m*-ITIC-based devices, its α value is 0.99 which is very close to 1, indicative of more efficient transportation of carriers and neglectable bimolecular recombination in the device. Typically, charge recombination is directly related with the FF of the devices. The lower bimolecular recombination in the *m*-ITIC-based PSCs agrees very well with the higher FF value of the *m*-ITIC-based devices (70.55%) relative to that (65.49%) of the ITIC-based devices. This observation is generally consistent with the relatively larger

DOI: 10.1021/jacs.6b09110
J. Am. Chem. Soc. 2016, 138, 15011−15018

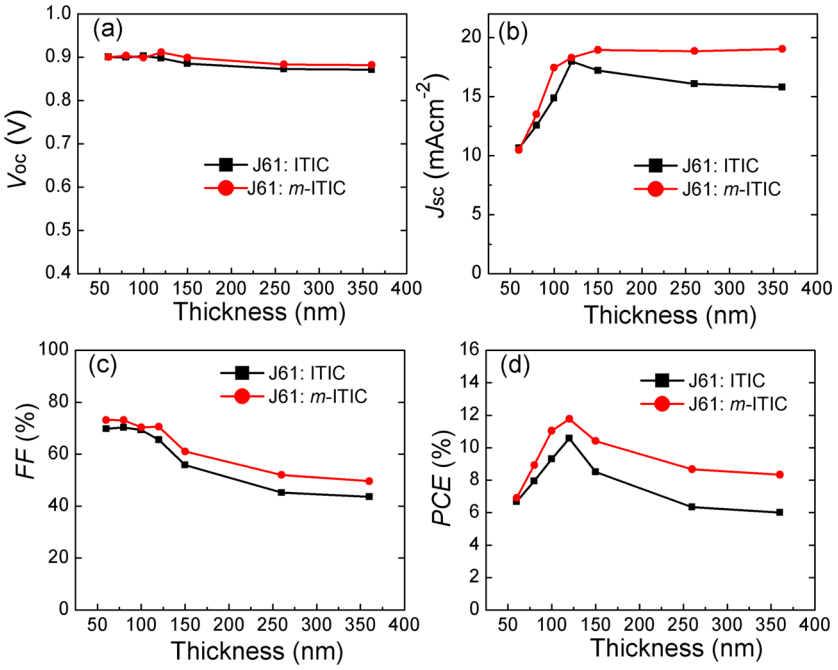

Figure 5. Effect of the active-layer thickness on the photovoltaic performance (J_{sc}, FF, V_{OC}, and PCE values) of the PSCs based on J61:ITIC or *m*-ITIC (1:1, w/w) with the active-layer thickness of 50−360 nm.

shunt resistance (R_{sh}) and smaller series resistance (R_s) values in the J61:*m*-ITIC-based devices (Table 2).

To gain more insights of the improved device performance by our side-chain engineering of the n-OS acceptor, the charge carriers mobilities of the active layers were estimated using the SCLC method,[64] and the measurement results are shown in Figure S3 in SI. For the J61:ITIC film, their hole (μ_h)/electron (μ_e) mobilities are estimated to be 2.07×10^{-4} cm^2 V^{-1} s^{-1}/1.05×10^{-4} cm^2 V^{-1} s^{-1} with μ_h/μ_e of 1.97, whereas for the J61:*m*-ITIC film, the corresponding hole/electron mobilities are 1.54×10^{-4} cm^2 V^{-1} s^{-1}/1.30×10^{-4} cm^2 V^{-1} s^{-1} with μ_h/μ_e of 1.18. The more balanced hole/electron mobilities inside the J61:*m*-ITIC film can partly account for the higher FF and higher PCE of the *m*-ITIC-based PSCs.[65]

Morphology Studies by GIWAXS and AFM. The aggregation morphologies[66] of the domains of the conjugated polymer donor and the n-OS acceptor in the active layers of the PSCs were studied by GIWAXS and AFM for further investigating the effect of the side-chain engineering of the acceptor on the photovoltaic performance of the nonfullerene PSCs. Figure 4a−c shows the results of the GIWAXS measurements of the J61:ITIC (1:1, w/w) and J61:*m*-ITIC (1:1, w/w) films. For the two blend films, the GIWAXS plots show more preferential face-on orientation, most especially for the J61:*m*-ITIC film. Also, semicrystalline structures with the diffraction patterns in both cases are contributed from individual components. The face-on orientation is desirable for higher charge carrier mobility. As mentioned above, the introduction of a side-chain on the *meta*-position of phenyl substituents of *m*-ITIC increased its self-organization behavior and crystallinity, so that it is true in its blend films with J61. In a comparison with those of the J61:ITIC film, diffraction patterns with significantly stronger peak intensity along with narrower peak width were observed for J61:*m*-ITIC samples (Figure 4a), suggesting that the crystalline content of the film was enhanced by the better defined scattering peak and intensities. All of these characteristics are associated with the higher crystalline behavior of the blend film, and are desirable for higher charge carrier mobility and therefore higher photovoltaic efficiencies, as discussed above.

The AFM height images based on five testing times on different areas for each samples show a root-mean-square (RMS) roughness of 0.899 ± 0.017 nm for J61:ITIC film and 1.097 ± 0.070 nm for J61:*m*-ITIC film. Representative AFM height images are shown in Figure 4d,e. The relatively smooth surface of the J61:ITIC and J61:*m*-ITIC blend film indicates good miscibility of the donor and acceptor components within their blend films, which was not disturbed by the semicrystalline characteristics of the donor and acceptor components. In addition, the slightly larger RMS values of the J61:*m*-ITIC film may be ascribed to its high semicrystallinity of *m*-ITIC. In the AFM phase images (see Figure 4f,g), both of the blend films show well-distributed nanofibrillar networks around tens of nanometers. Notably, the more preferred domain size of ∼15 nm in the J61:*m*-ITIC blend certainly accounts for its observed superior device performance.

Thickness Dependence of the Photovoltaic Performance. The high photovoltaic performance with thickness-insensitive behavior in the range 100−300 nm for the active-layer thickness is crucial for large area fabrication toward future application of the PSCs. Therefore, the thickness-insensitive photovoltaic performance of high efficiency conjugated polymer donor materials in the fullerene-based PSCs have attracted attention in recent years.[7,67−69] However, there are seldom reports on the thickness-insensitive photovoltaic performance of the nonfullerene PSCs. Herein, we studied the effect of active-layer thickness on the photovoltaic performance of the PSCs based on J61:ITIC and J61:*m*-ITIC in the active-layer thickness range 60−360 nm. Tables S1 and S2 in SI list the photovoltaic parameters of the devices with different active-layer thicknesses, and Figure 5 shows the active-layer thickness dependence of the photovoltaic parameters of V_{oc}, J_{sc}, FF, and PCE values. V_{oc} values are nearly constant for the two devices in the whole thickness range, with a small

DOI: 10.1021/jacs.6b09110
J. Am. Chem. Soc. 2016, 138, 15011−15018

decrease for the active layers of the devices thicker than 120 nm (see Figure 5a). In contrast, the J_{sc} and FF values show significant thickness-dependent behavior for the two devices. For the J61:*m*-ITIC device, with the increase of the active-layer thickness from 60 to 120 nm, J_{sc} increases greatly from 10.68 mA cm^{-2} at 60 nm to 18.31 mA cm^{-2} at 120 nm (Table S2 in SI). With further increase of the active-layer thickness over 120 nm, J_{sc} remains at a high value with a slight increase to 19.04 mA cm^{-2} at a thickness of 360 nm (see Figure 5b and Table S2 in SI). However, for the J61:ITIC device, its J_{sc} reached a peak value of 17.97 mA cm^{-2} at the thickness of 120 nm and then decreased with a further increase of the active-layer thickness (Figure 5b). Actually, the thickness dependence of J_{sc} is a trade-off between absorbance and charge recombination; the thicker active layer will enhance absorbance which is beneficial to higher J_{sc}, but it also increases charge recombination opportunity which will decrease J_{sc}. The different behavior of the J_{sc} values for the two devices at thicker active layers further confirms that the charge recombination in the *m*-ITIC-based device is much less than that in the ITIC-based device. The slowly dropping trend in FF values of the two devices, as shown in Figure 5c, could be due to the increased series resistance of the devices with the increase in the active-layer thickness.

In combination with the thickness dependence of the V_{oc}, J_{sc}, and FF values, the thickness dependence of PCE is dominated by that of J_{sc} in the thickness range from 60 to 120 nm and then controlled by that of FF from 120 to 360 nm (see Figure 5d). For the PSCs based on J61:*m*-ITIC, the maximum PCE is 11.77% at the active-layer thickness of 120 nm, then with the increase of the active-layer thickness, the PCE values decreased gradually. Nevertheless, only limited PCE decrease was observed until the thickness increased to 360 nm. The PCE is still over 8.50% (73% of the peak value) for the device with an active-layer thickness of 260 nm and over 8.00% (68% of the peak value) at the thickness of 360 nm (Figure 5d and Table S2 in SI). While for the PSCs based on J61:ITIC, more dramatic decrease in PCE can be seen; PCE values at 260 and 360 nm are 6.34% and 6.0%, respectively, corresponding to 60% and 57% of its peak value. The less thickness-dependent photovoltaic performance of the J61:*m*-ITIC-based device should benefit from the high electron mobility of *m*-ITIC and less charge recombination in the blend of J61:*m*-ITIC. The results indicate that subtle side-chain engineering on n-OSs can help to realize thickness-insensitive photovoltaic devices. The good and thickness-insensitive photovoltaic performance of the J61:*m*-ITIC-based PSCs should be promising for large area fabrication and future applications of the PSCs.

CONCLUSION

By side-chain isomerism engineering on the alkyl-phenyl substituents of ITIC, a new low bandgap n-OS *m*-ITIC with *meta*-alkyl-phenyl substituents was synthesized and characterized. *m*-ITIC demonstrated a more crystalline and stronger film absorption coefficient, slightly (ca. 0.02 eV) upshifted LUMO and HOMO energy levels, and greater electron motility in comparison with its isomer ITIC with a *para*-alkyl-phenyl substituent. Nonfullerene PSCs with *m*-ITIC as acceptor and a medium bandgap conjugated polymer J61 as donor demonstrated a high PCE of 11.77% with a V_{OC} of 0.912 V, a J_{sc} of 18.31 mA/cm^2, and an FF of 70.55%, which is significantly improved over the PCE of 10.57% for the corresponding ITIC-based device under the same experimental conditions. More importantly, *m*-ITIC-based devices show less thickness dependence of the photovoltaic performance on active-layer thickness, and the PCE of the devices is still over 8.50% with an active-layer thickness of 250 nm and over 8.00% at the thickness of 360 nm, which is beneficial for large area device fabrication. These results indicate that *m*-ITIC is a promising low bandgap n-OS acceptor for nonfullerene PSCs and the side-chain isomerization could be an easy and convenient way to further improve the photovoltaic performance of the donor and acceptor materials for high efficiency PSCs.

ASSOCIATED CONTENT

Supporting Information

The Supporting Information is available free of charge on the ACS Publications website at DOI: 10.1021/jacs.6b09110.

Synthetic route of *m*-ITIC, TGA plots of ITIC and *m*-ITIC, and the effect of the active-layer thickness on the photovoltaic performance of the PSCs (PDF)

AUTHOR INFORMATION

Corresponding Authors

*zgzhangwhu@iccas.ac.cn

*liyf@iccas.ac.cn

Notes

The authors declare no competing financial interest.

ACKNOWLEDGMENTS

The work was supported by the Ministry of Science and Technology of China (973 project, no. 2014CB643501) and NSFC (nos. 91433117, 91333204, and 21374124) and the Strategic Priority Research Program of the Chinese Academy of Sciences, Grant XDB12030200.

REFERENCES

(1) Yu, G.; Gao, J.; Hummelen, J. C.; Wudl, F.; Heeger, A. J. *Science* **1995**, *270*, 1789−1791.
(2) Thompson, B. C.; Fréchet, J. M. J. *Angew. Chem., Int. Ed.* **2008**, *47*, 58−77.
(3) Li, G.; Zhu, R.; Yang, Y. *Nat. Photonics* **2012**, *6*, 153−161.
(4) Huang, Y.; Kramer, E. J.; Heeger, A. J.; Bazan, G. C. *Chem. Rev.* **2014**, *114*, 7006−7043.
(5) Li, C.; Liu, M.; Pschirer, N. G.; Baumgarten, M.; Müllen, K. *Chem. Rev.* **2010**, *110*, 6817−6855.
(6) Liu, Y.; Zhao, J.; Li, Z.; Mu, C.; Ma, W.; Hu, H.; Jiang, K.; Lin, H.; Ade, H.; Yan, H. *Nat. Commun.* **2014**, *5*, 5293.
(7) Zhao, J.; Li, Y.; Yang, G.; Jiang, K.; Lin, H.; Ade, H.; Ma, W.; Yan, H. *Nature Energy* **2016**, *1*, 15027.
(8) He, Z.; Xiao, B.; Liu, F.; Wu, H.; Yang, Y.; Xiao, S.; Wang, C.; Russell, T. P.; Cao, Y. *Nat. Photonics* **2015**, *9*, 174−179.
(9) Liao, S. H.; Jhuo, H. J.; Yeh, P. N.; Cheng, Y. S.; Li, Y. L.; Lee, Y. H.; Sharma, S.; Chen, S. A. *Sci. Rep.* **2014**, *4*, 6813.
(10) Zhang, S.; Ye, L.; Zhao, W.; Yang, B.; Wang, Q.; Hou, J. *Sci. China: Chem.* **2015**, *58*, 248−256.
(11) Long, X.; Ding, Z.; Dou, C.; Zhang, J.; Liu, J.; Wang, L. *Adv. Mater.* **2016**, *28*, 6504−6508.
(12) Zhan, X.; Tan, Z. a.; Domercq, B.; An, Z.; Zhang, X.; Barlow, S.; Li, Y.; Zhu, D.; Kippelen, B.; Marder, S. R. *J. Am. Chem. Soc.* **2007**, *129*, 7246−7247.
(13) Zhou, E.; Cong, J.; Wei, Q.; Tajima, K.; Yang, C.; Hashimoto, K. *Angew. Chem., Int. Ed.* **2011**, *50*, 2799−2803.
(14) Zhou, Y.; Kurosawa, T.; Ma, W.; Guo, Y. K.; Fang, L.; Vandewal, K.; Diao, Y.; Wang, C. G.; Yan, Q. F.; Reinspach, J.; Mei, J. G.; Appleton, A. L.; Koleilat, G. I.; Gao, Y. L.; Mannsfeld, S. C. B.; Salleo, A.; Ade, H.; Zhao, D. H.; Bao, Z. N. *Adv. Mater.* **2014**, *26*, 3767−3772.
(15) Yan, H.; Chen, Z.; Zheng, Y.; Newman, C.; Quinn, J. R.; Dotz, F.; Kastler, M.; Facchetti, A. *Nature* **2009**, *457*, 679−686.

DOI: 10.1021/jacs.6b09110
J. Am. Chem. Soc. 2016, 138, 15011−15018

(16) Lee, C.; Kang, H.; Lee, W.; Kim, T.; Kim, K.-H.; Woo, H. Y.; Wang, C.; Kim, B. J. *Adv. Mater.* **2015**, *27*, 2466−2471.
(17) Hwang, Y.-J.; Courtright, B. A. E.; Ferreira, A. S.; Tolbert, S. H.; Jenekhe, S. A. *Adv. Mater.* **2015**, *27*, 4578−4584.
(18) Jung, J. W.; Jo, J. W.; Chueh, C.-C.; Liu, F.; Jo, W. H.; Russell, T. P.; Jen, A. K. Y. *Adv. Mater.* **2015**, *27*, 3310−3317.
(19) Li, Z.; Xu, X.; Zhang, W.; Meng, X.; Ma, W.; Yartsev, A.; Inganäs, O.; Andersson, M. R.; Janssen, R. A. J.; Wang, E. *J. Am. Chem. Soc.* **2016**, *138*, 10935−10944.
(20) Nakano, K.; Nakano, M.; Xiao, B.; Zhou, E.; Suzuki, K.; Osaka, I.; Takimiya, K.; Tajima, K. *Macromolecules* **2016**, *49*, 1752−1760.
(21) Nielsen, C. B.; Holliday, S.; Chen, H.-Y.; Cryer, S. J.; McCulloch, I. *Acc. Chem. Res.* **2015**, *48*, 2803−2812.
(22) Holliday, S.; Ashraf, R. S.; Nielsen, C. B.; Kirkus, M.; Röhr, J. A.; Tan, C.-H.; Collado-Fregoso, E.; Knall, A.-C.; Durrant, J. R.; Nelson, J.; McCulloch, I. *J. Am. Chem. Soc.* **2015**, *137*, 898−904.
(23) Holliday, S.; Ashraf, R. S.; Wadsworth, A.; Baran, D.; Yousaf, S. A.; Nielsen, C. B.; Tan, C.-H.; Dimitrov, S. D.; Shang, Z.; Gasparini, N.; Alamoudi, M.; Laquai, F.; Brabec, C. J.; Salleo, A.; Durrant, J. R.; McCulloch, I. *Nat. Commun.* **2016**, *7*, 11585.
(24) Hartnett, P. E.; Timalsina, A.; Matte, H. S. S. R.; Zhou, N.; Guo, X.; Zhao, W.; Facchetti, A.; Chang, R. P. H.; Hersam, M. C.; Wasielewski, M. R.; Marks, T. J. *J. Am. Chem. Soc.* **2014**, *136*, 16345−16356.
(25) Zhang, X.; Lu, Z.; Ye, L.; Zhan, C.; Hou, J.; Zhang, S.; Jiang, B.; Zhao, Y.; Huang, J.; Zhang, S.; Liu, Y.; Shi, Q.; Liu, Y.; Yao, J. *Adv. Mater.* **2013**, *25*, 5791−5797.
(26) Meng, D.; Sun, D.; Zhong, C.; Liu, T.; Fan, B.; Huo, L.; Li, Y.; Jiang, W.; Choi, H.; Kim, T.; Kim, J. Y.; Sun, Y.; Wang, Z.; Heeger, A. J. *J. Am. Chem. Soc.* **2016**, *138*, 375−380.
(27) Zhong, Y.; Trinh, M. T.; Chen, R.; Purdum, G. E.; Khlyabich, P. P.; Sezen, M.; Oh, S.; Zhu, H.; Fowler, B.; Zhang, B.; Wang, W.; Nam, C.-Y.; Sfeir, M. Y.; Black, C. T.; Steigerwald, M. L.; Loo, Y.-L.; Ng, F.; Zhu, X. Y.; Nuckolls, C. *Nat. Commun.* **2015**, *6*, 8242.
(28) Hartnett, P. E.; Matte, H. S. S. R.; Eastham, N. D.; Jackson, N. E.; Wu, Y.; Chen, L. X.; Ratner, M. A.; Chang, R. P. H.; Hersam, M. C.; Wasielewski, M. R.; Marks, T. J. *Chemical Science* **2016**, *7*, 3543−3555.
(29) Liu, Y.; Mu, C.; Jiang, K.; Zhao, J.; Li, Y.; Zhang, L.; Li, Z.; Lai, J. Y. L.; Hu, H.; Ma, T.; Hu, R.; Yu, D.; Huang, X.; Tang, B. Z.; Yan, H. *Adv. Mater.* **2015**, *27*, 1015−1020.
(30) Zhong, H.; Wu, C.-H.; Li, C.-Z.; Carpenter, J.; Chueh, C.-C.; Chen, J.-Y.; Ade, H.; Jen, A. K. Y. *Adv. Mater.* **2016**, *28*, 951−958.
(31) Wu, Q.; Zhao, D.; Schneider, A. M.; Chen, W.; Yu, L. *J. Am. Chem. Soc.* **2016**, *138*, 7248−7251.
(32) Kwon, O. K.; Uddin, M. A.; Park, J.-H.; Park, S. K.; Nguyen, T. L.; Woo, H. Y.; Park, S. Y. *Adv. Mater.* **2016**, *28*, 910−916.
(33) Li, H.; Earmme, T.; Ren, G.; Saeki, A.; Yoshikawa, S.; Murari, N. M.; Subramaniyan, S.; Crane, M. J.; Seki, S.; Jenekhe, S. A. *J. Am. Chem. Soc.* **2014**, *136*, 14589−14597.
(34) Li, H.; Hwang, Y.-J.; Courtright, B. A. E.; Eberle, F. N.; Subramaniyan, S.; Jenekhe, S. A. *Adv. Mater.* **2015**, *27*, 3266−3272.
(35) Wu, X. F.; Fu, W. F.; Xu, Z.; Shi, M. M.; Liu, F.; Chen, H. Z.; Wan, J. H.; Russell, T. P. *Adv. Funct. Mater.* **2015**, *25*, 5954−5966.
(36) Li, S.; Liu, W.; Shi, M.; Mai, J.; Lau, T.-K.; Wan, J.; Lu, X.; Li, C.-Z.; Chen, H. *Energy Environ. Sci.* **2016**, *9*, 604−610.
(37) Josse, P.; Dalinot, C.; Jiang, Y.; Dabos-Seignon, S.; Roncali, J.; Blanchard, P.; Cabanetos, C. *J. Mater. Chem. A* **2016**, *4*, 250−256.
(38) Lin, Y.; Wang, J.; Zhang, Z.-G.; Bai, H.; Li, Y.; Zhu, D.; Zhan, X. *Adv. Mater.* **2015**, *27*, 1170−1174.
(39) Gao, L.; Zhang, Z.-G.; Xue, L.; Min, J.; Zhang, J.; Wei, Z.; Li, Y. *Adv. Mater.* **2016**, *28*, 1884−1890.
(40) Li, S.; Ye, L.; Zhao, W.; Zhang, S.; Mukherjee, S.; Ade, H.; Hou, J. *Adv. Mater.* **2016**, DOI: 10.1002/adma.201602776.
(41) Facchetti, A. *Mater. Today* **2013**, *16*, 123−132.
(42) Zhao, W.; Qian, D.; Zhang, S.; Li, S.; Inganäs, O.; Gao, F.; Hou, J. *Adv. Mater.* **2016**, *28*, 4734−4739.
(43) Bin, H.; Zhang, Z.-G.; Gao, L.; Chen, S.; Zhong, L.; Xue, L.; Yang, C.; Li, Y. *J. Am. Chem. Soc.* **2016**, *138*, 4657−4664.
(44) Gao, L.; Zhang, Z.-G.; Bin, H.; Xue, L.; Yang, Y.; Wang, C.; Liu, F.; Russell, T. P.; Li, Y. *Adv. Mater.* **2016**, *28*, 8288−8295.
(45) Li, Y.; Liu, X.; Wu, F.-P.; Zhou, Y.; Jiang, Z.-Q.; Song, B.; Xia, Y.; Zhang, Z.-G.; Gao, F.; Inganas, O.; Li, Y.; Liao, L.-S. *J. Mater. Chem. A* **2016**, *4*, 5890−5897.
(46) Lin, Y.; Zhang, Z.-G.; Bai, H.; Wang, J.; Yao, Y.; Li, Y.; Zhu, D.; Zhan, X. *Energy Environ. Sci.* **2015**, *8*, 610−616.
(47) Wu, Y.; Bai, H.; Wang, Z.; Cheng, P.; Zhu, S.; Wang, Y.; Ma, W.; Zhan, X. *Energy Environ. Sci.* **2015**, *8*, 3215−3221.
(48) Lin, Y.; Zhao, F.; He, Q.; Huo, L.; Wu, Y.; Parker, T. C.; Ma, W.; Sun, Y.; Wang, C.; Zhu, D.; Heeger, A. J.; Marder, S. R.; Zhan, X. *J. Am. Chem. Soc.* **2016**, *138*, 4955−4961.
(49) Zhang, Z.-G.; Li, Y. *Sci. China: Chem.* **2015**, *58*, 192−209.
(50) Graham, K. R.; Cabanetos, C.; Jahnke, J. P.; Idso, M. N.; El Labban, A.; Ngongang Ndjawa, G. O.; Heumueller, T.; Vandewal, K.; Salleo, A.; Chmelka, B. F.; Amassian, A.; Beaujuge, P. M.; McGehee, M. D. *J. Am. Chem. Soc.* **2014**, *136*, 9608−9618.
(51) Cabanetos, C.; El Labban, A.; Bartelt, J. A.; Douglas, J. D.; Mateker, W. R.; Fréchet, J. M. J.; McGehee, M. D.; Beaujuge, P. M. *J. Am. Chem. Soc.* **2013**, *135*, 4656−4659.
(52) Chen, M. S.; Lee, O. P.; Niskala, J. R.; Yiu, A. T.; Tassone, C. J.; Schmidt, K.; Beaujuge, P. M.; Onishi, S. S.; Toney, M. F.; Zettl, A.; Fréchet, J. M. J. *J. Am. Chem. Soc.* **2013**, *135*, 19229−19236.
(53) Lei, T.; Wang, J.-Y.; Pei, J. *Chem. Mater.* **2014**, *26*, 594−603.
(54) Mei, J.; Bao, Z. *Chem. Mater.* **2014**, *26*, 604−615.
(55) Yang, L.; Tumbleston, J. R.; Zhou, H.; Ade, H.; You, W. *Energy Environ. Sci.* **2013**, *6*, 316−326.
(56) Dang, D.; Chen, W.; Himmelberger, S.; Tao, Q.; Lundin, A.; Yang, R.; Zhu, W.; Salleo, A.; Müller, C.; Wang, E. *Adv. Energy Mater.* **2014**, *4*, 1400680.
(57) Josse, P.; Labrunie, A.; Dalinot, C.; McAfee, S. M.; Dabos-Seignon, S.; Roncali, J.; Welch, G. C.; Blanchard, P.; Cabanetos, C. *Org. Electron.* **2016**, *37*, 479−484.
(58) Xu, X.; Li, Z.; Backe, O.; Bini, K.; James, D. I.; Olsson, E.; Andersson, M. R.; Wang, E. *J. Mater. Chem. A* **2014**, *2*, 18988−18997.
(59) Li, Y. F.; Cao, Y.; Gao, J.; Wang, D.; Yu, G.; Heeger, A. J. *Synth. Met.* **1999**, *99*, 243−248.
(60) Sun, Q.; Wang, H.; Yang, C.; Li, Y. *J. Mater. Chem.* **2003**, *13*, 800−806.
(61) Rivnay, J.; Mannsfeld, S. C. B.; Miller, C. E.; Salleo, A.; Toney, M. F. *Chem. Rev.* **2012**, *112*, 5488−5519.
(62) Zhang, Z.-G.; Qi, B.; Jin, Z.; Chi, D.; Qi, Z.; Li, Y.; Wang, J. *Energy Environ. Sci.* **2014**, *7*, 1966−1973.
(63) Schilinsky, P.; Waldauf, C.; Brabec, C. J. *Appl. Phys. Lett.* **2002**, *81*, 3885−3887.
(64) Malliaras, G. G.; Salem, J. R.; Brock, P. J.; Scott, C. *Phys. Rev. B: Condens. Matter Mater. Phys.* **1998**, *58*, R13411−R13414.
(65) Bartesaghi, D.; Perez, I. d. C.; Kniepert, J.; Roland, S.; Turbiez, M.; Neher, D.; Koster, L. J. A. *Nat. Commun.* **2015**, *6*, 7083.
(66) Liu, F.; Gu, Y.; Shen, X.; Ferdous, S.; Wang, H.-W.; Russell, T. P. *Prog. Polym. Sci.* **2013**, *38*, 1990−2052.
(67) Price, S. C.; Stuart, A. C.; Yang, L.; Zhou, H.; You, W. *J. Am. Chem. Soc.* **2011**, *133*, 4625−4631.
(68) Li, W.; Hendriks, K. H.; Roelofs, W. S. C.; Kim, Y.; Wienk, M. M.; Janssen, R. A. J. *Adv. Mater.* **2013**, *25*, 3182−3186.
(69) Hu, X.; Yi, C.; Wang, M.; Hsu, C.-H.; Liu, S.; Zhang, K.; Zhong, C.; Huang, F.; Gong, X.; Cao, Y. *Adv. Energy Mater.* **2014**, *4*, 1400378.

DOI: 10.1021/jacs.6b09110
J. Am. Chem. Soc. 2016, 138, 15011−15018